ANESTHESIOLOGY®

Hippocampal Neural Dynamics and Postoperative Delirium–like Behavior in Aged Mice

Shiqi Guo, Ph.D., Liuyue Yang, M.D., Weihua Ding, M.D., Tewodros Mulugeta Dagnew, Ph.D., Yuting Gao, M.D., Wei Wang, M.D., Pei Wang, Ph.D., Song Huang, M.D., Chongzhao Ran, Ph.D., Changning Wang, Ph.D., Le Shen, M.D., Ph.D., Qian Chen, Ph.D., Oluwaseun Akeju, M.D., Shiqian Shen, M.D.

ANESTHESIOLOGY 2025; 143:625–40

EDITOR'S PERSPECTIVE

What We Already Know about This Topic

- Postoperative delirium is an important clinical entity, especially in at-risk populations
- The electroencephalographic features of postoperative delirium are incompletely characterized

What This Article Tells Us That Is New

- In aged mice, the combination of anesthesia/surgery decreased hippocampal interneuron activity and increased pyramidal neuron activity, as demonstrated by high-density silicon probe electrophysiologic recordings and *in vivo* calcium imaging
- Pretreatment of mice before anesthesia and surgery with indole-3-proprionic acid, a gut microbiome metabolite, mitigated the development of postoperative delirium–like behavior, and these protective behavioral effects were correlated with the absence of changes in excitation inhibition balance when compared to control animals

ABSTRACT

Background: Postoperative delirium (POD) is a common and serious clinical condition that occurs after anesthesia/surgery. While its clinical impact is well recognized, the underlying electrophysiologic mechanisms remain largely unknown, posing challenges for effective treatment. This study aims to investigate hippocampal neural dynamics before and after anesthesia/surgery in aged mice, which have a tendency to develop POD.

Methods: This study included adult and aged mice with a POD model. POD-like behavior was assessed in N = 10 mice at baseline (the day before surgery), as well as at 9 h and 24 h after anesthesia/surgery. A behavioral battery, including the open field test, Y maze, buried food test, and novel object recognition, was used for assessment. *In vivo* chronic brain recordings were performed on awake, restrained mice using a high-density silicon probe during the same time intervals. To further investigate hippocampal neural dynamics, *in vivo* two-photon calcium imaging was also conducted. Additionally, aged mice were pretreated with indole-3-propionic acid (IPA), and its effects on POD-like behavior and neural activity were evaluated using electrophysiology and calcium imaging.

Results: The first observation was that aged mice exhibited significant POD-like behavior, as measured by Z scores, compared to adult mice after anesthesia/surgery. Analysis revealed significant age-related differences in hippocampal neuronal activities. At 9 h after surgery, aged mice exhibited a marked increase in pyramidal cell activity and a reduction in interneuron activity compared to adult mice. These changes in neuronal dynamics were associated with the onset of POD-like symptoms in aged mice. By 24 h after surgery, both pyramidal cell and interneuron activity in aged mice had returned to presurgery levels, which coincided with an improvement in POD-like behavior. Additionally, IPA pretreatment modulated neuronal activity in aged mice, attenuating pyramidal cell hyperactivity and partially ameliorating interneuron dysfunction, changes associated with mitigated POD-like behavior.

Conclusions: Alterations in hippocampal neural activity may significantly contribute to brain dysfunction and POD-like behavior. IPA pretreatment may modulate neural circuit imbalances in aged mice, potentially mitigating POD incidence.

(ANESTHESIOLOGY 2025; 143:625–40)

Several serious cognitive syndromes can emerge after surgery and anesthesia. Postoperative delirium (POD) is a behavioral disorder that occurs during the perioperative period, marked

This article is featured in "This Month in ANESTHESIOLOGY," page A1. This article is accompanied by an editorial on p. 496. This article has a related Infographic on p. A18. Supplemental Digital Content is available for this article. Direct URL citations appear in the printed text and are available in both the HTML and PDF versions of this article. Links to the digital files are provided in the HTML text of this article on the Journal's Web site (www.anesthesiology.org). This article has a video abstract. This article has an audio podcast. S.Q. and L.Y. contributed equally to this work.

Submitted for publication October 23, 2024. Accepted for publication March 25, 2025. Published online first on March 28, 2025.

Shiqi Guo, Ph.D.: Department of Anesthesia, Critical Care and Pain Medicine, Massachusetts General Hospital and Harvard Medical School, Charlestown, Massachusetts.

 ANESTHESIOLOGY 2025; 143:625–40. DOI: 10.1097/ALN.0000000000005478

Abbreviations: **EEG**, electroencephalogram; **HSP**, high-density silicon probe; **IPA**, indole-3-propionic acid; **NOR**, novel object recognition; **POD**, postoperative delirium

<zdoi;10.1097/ALN.0000000000005478>

by impaired consciousness and cognitive dysfunction.[1,2] The incidence of POD is relatively low in the general surgical population (2 to 3%), but it rises significantly in high-risk patients, reaching as high as 50%.[3–5] Clinical studies have identified several risk factors for POD, including advanced age, preexisting dementia, being underweight, lower educational levels, smoking, and a history of delirium.[6,7] These risk factors contribute to a higher incidence of POD in certain populations. Among older adults, the incidence is particularly high, affecting 9 to 50% of cases. In this group, POD is associated with worse clinical outcomes, including increased postoperative complications, prolonged hospital stays, and higher mortality rates.[8–11] The healthcare costs attributable to postoperative delirium are estimated at $32.9 billion per year.[12]

Electroencephalogram (EEG) studies have provided insights into brain electrophysiologic activity in POD. While EEG features of delirium in the postoperative period remain incompletely characterized, a shift of EEG power into low frequencies is a typical finding shared among encephalopathies that manifest with delirium.[13–15] During loss of consciousness after the induction of general anesthesia, POD patients demonstrated decreased alpha and beta band power, as well as lower spectral edge frequencies, than patients without POD.[16] Preoperative awake, resting EEG alpha attenuation with eye opening was associated with the development of POD.[17] The predictive value of preoperative EEG was independently validated, particularly when combining resting state EEG and Montreal Cognitive Assessment scores (Ning M, Rodionov A, Ross JM, et al.: Prediction of post-operative delirium in older adults from preoperative cognition and alpha power from resting-state EEG. Preprint. Posted online November 1, 2024. doi:10.1101/2024.08.15.24312053). More recently, using high-density EEG, it was shown that delirium was associated with loss of feedback cortical activity.[18] However, in a recent study of older adults who underwent cardiac surgery, intraoperative EEG-guided anesthesia management to minimize burst suppression did not decrease the incidence of POD in these patients,[19] highlighting the complexity of POD pathogenesis.

Despite significant progress to link brain electrical activities and POD, the detailed electrophysiologic basis of POD is largely unknown. While seminal studies based on EEG identify important features with predictive power for POD, brain region– or neuron-specific information is not readily available due to the limited spatial resolution of EEG. The advent of high-density silicon probes (HSP), such as the Neuropixels 2.0 (IMEC, Belgium), offers a breakthrough in this regard. These miniaturized, high-density probes enable stable, long-term chronic brain recordings with single-unit resolution, while their high-density, multishank design facilitates precise localization of single-unit neural activity across different brain regions.[20] For example, the 5,120 recording sites across four shanks in these probes have been shown to track individual chronically recorded neurons in the primary visual cortex with a greater than 80% success rate for up to 2 months.[20] Despite the enthusiastic adoption of this technology within the neuroscience community,[21,22] *in vivo* high-density electrophysiologic studies with single-unit resolution have yet to be applied to understanding neuronal activity linked to POD.

In the current study, we first analyzed POD-like behavior in aged mice compared to adult mice. We then utilized high-density single-unit chronic electrophysiologic recording technology to capture single-unit electrophysiologic signals in the hippocampus of both adult and aged mice, while intravital two-photon calcium imaging was conducted in separate cohorts of animals, enabling direct visualization of neuronal activity. Building on our previous retrospective study, we demonstrated that indole-3-propionic acid (IPA), a gut microbiome metabolite,[23] effectively prevented POD in aged mice. This occurred through the promotion of PGC-1α expression in hippocampal interneurons, which protects against POD development linked to gut microbiota perturbation.[24] In this study, we aimed to further investigate the impact of IPA on hippocampal neural activity. Specifically, we hypothesized that dynamic changes in neural activity could be recorded in a model of POD-like behavior and that IPA modulates hippocampal neural activity to mitigate the disruptions associated with POD.

Liuyue Yang, M.D.: Department of Anesthesia, Critical Care and Pain Medicine, Massachusetts General Hospital and Harvard Medical School, Charlestown, Massachusetts.

Weihua Ding, M.D.: Department of Anesthesia, Critical Care and Pain Medicine, Massachusetts General Hospital and Harvard Medical School, Charlestown, Massachusetts.

Tewodros Mulugeta Dagnew, Ph.D.: Massachusetts General Hospital/Harvard-MIT Health Sciences and Technology Martinos Center for Biomedical Imaging, Department of Radiology, Massachusetts General Hospital, Harvard Medical School, Charlestown, Massachusetts.

Yuting Gao, M.D.: Department of Anesthesia, Critical Care and Pain Medicine, Massachusetts General Hospital and Harvard Medical School, Charlestown, Massachusetts.

Wei Wang, M.D.: Department of Anesthesia, Critical Care and Pain Medicine, Massachusetts General Hospital and Harvard Medical School, Charlestown, Massachusetts.

Pei Wang, Ph.D.: Department of Anesthesia, Critical Care and Pain Medicine, Massachusetts General Hospital and Harvard Medical School, Charlestown, Massachusetts.

Song Huang, M.D.: Department of Anesthesia, Critical Care and Pain Medicine, Massachusetts General Hospital and Harvard Medical School, Charlestown, Massachusetts.

Chongzhao Ran, Ph.D.: Massachusetts General Hospital/Harvard-MIT Health Sciences and Technology Martinos Center for Biomedical Imaging, Department of Radiology, Massachusetts General Hospital, Harvard Medical School, Charlestown, Massachusetts.

Changning Wang, Ph.D.: Massachusetts General Hospital/Harvard-MIT Health Sciences and Technology Martinos Center for Biomedical Imaging, Department of Radiology, Massachusetts General Hospital, Harvard Medical School, Charlestown, Massachusetts.

Le Shen, M.D. Ph.D.: Department of Anesthesia, Peking Union Hospital, Chinese Academy of Medical Sciences, Dongcheng District, Beijing, China

Qian Chen, Ph.D.: Zhongshan Institute for Drug Discovery, Shanghai Institute of Materia Medica, SSIP Healthcare and Medicine Demonstration Zone, Zhongshan Tsuihang New District, Guangdong, China

Oluwaseun Akeju, M.D.: Department of Anesthesia, Critical Care and Pain Medicine, Massachusetts General Hospital and Harvard Medical School, Charlestown, Massachusetts.

Shiqian Shen, M.D.: Department of Anesthesia, Critical Care and Pain Medicine, Massachusetts General Hospital and Harvard Medical School, Charlestown, Massachusetts.

Materials and Methods

Animals

All experiments conducted in this study adhered to the guidelines and regulations set by the National Institutes of Health (Bethesda, Maryland) and were approved by the Institutional Animal Care and Use Committee at Massachusetts General Hospital (Charlestown, Massachusetts). The study involved adult male and female C57BL/6 mice aged 12 to 16 weeks and aged male and female C57BL/6 mice aged 17 to 18 months at the start of the experiment. Every effort was made to minimize the number of animals used. The mice were obtained from the Jackson Laboratory (USA) and housed in a temperature-controlled environment with a 12-h light/12-h dark cycle (lights on at 7:00 AM and off at 7:00 PM), with behavioral testing carried out during the light phase. The mice had access to food and water *ad libitum*. The animal care and monitoring procedures adhered to the Animals in Research: Reporting In Vivo Experiments (ARRIVE) guidelines to ensure transparent reporting. Protocols were implemented to minimize pain, suffering, and distress, and all adverse events, whether anticipated or unexpected, were recorded. Humane endpoints were established, and specific signs, along with their frequency, were closely monitored throughout the study.

Anesthesia/Surgery Procedure of Postoperative Delirium Model

The procedure was performed as previously described.[24] Briefly, the mice were anesthetized using oxygenated isoflurane (3% for induction and 1.5% for maintenance) delivered in oxygen.[25,26] We used a mice model imitating femoral artery surgery,[24] as this surgery is widely used clinically. During the procedure, the mice were placed on a heating pad to ensure their body temperature was maintained, and eye ointment was applied to prevent corneal dryness. The mice were positioned in a supine posture, and the hair on both side of the hind limb was shaved. A small incision, approximately 0.5 cm in length, was made in the skin over the femoral artery, extending from the inguinal region down toward the knee. The subcutaneous tissue and fascia were carefully dissected to expose the bilateral femoral arteries, taking great care to avoid any damage to the surrounding tissues and nerves. Exposure of the artery was performed using a mini forceps, ensuring the artery remained intact to prevent bleeding. The skin incision was closed using 4-0 silk sutures. The total duration of anesthesia and surgery was 2 h for all mice. For sham procedures, animals underwent isoflurane anesthesia for similar duration, but no incision was made. For immediate postoperative pain management, the skin was infiltrated with 0.25% bupivacaine, and the wound was covered with EMLA cream (AstraZeneca, USA). For IPA intraperitoneal injection, IPA was dissolved in 0.9% NaCl:ethanol (v/v 10:1) and injected twice daily at 0.0625 mmol/kg.

Open Field Test

The mice were acclimated for approximately 30 min before testing began. The test was conducted in a 40-cm × 40-cm enclosure, which was divided into two sections: a center zone measuring 20 cm × 20 cm, and a surrounding area. The movements of the mice were recorded and analyzed using a video camera connected to the Any-Maze animal tracking system (Stoelting Co., USA). Each mouse was placed individually in the center of the enclosure, and various parameters were measured, including the time taken to enter the center zone, the duration spent in the center zone, and the amount of time spent freezing. The open field test lasted for 5 min.

Y Maze Test

The Y maze test was used to assess spontaneous alternation behavior and short-term spatial memory in mice. The Y maze apparatus featured three arms arranged at 120° angles, all connected at a central zone. Before testing, the mice were acclimated to the environment for 5 to 10 min. A video camera was positioned vertically above the Y maze to capture the movement of each mouse. The live tracking data were recorded and analyzed using the Any-Maze animal tracking system software (Stoelting Co.). Key metrics included the number of entries into the novel arm and the amount of time spent in the novel arm.

Buried Food Test

The buried food test was conducted to evaluate the alertness and consciousness of the mice, following a previously described protocol with slight modifications.[27,28] Two days before the test, the mice were introduced to sweetened cereal. On the day of the test, after acclimation, each mouse was placed in a clean cage where a sweetened cereal pellet had been buried under 3 to 5 cm of bedding. The time it took for the mouse to find and eat the buried food was recorded.

Novel Object Recognition

The novel object recognition (NOR) test was used to assess recognition memory in mice. Briefly, the mice were placed in a 40-cm × 40-cm enclosure, and their exploration of the objects was recorded using the Any-Maze animal tracking system (Stoelting Co.). The mice were placed in the center of the enclosure and allowed to explore two similar identical objects for 10 min, after which they were returned to their home cage to rest for 10 min. Subsequently, one of the two objects was replaced with a novel object, and the mice were placed back into the enclosure and tested for another 10 min. The exploration time for each object was recorded for statistical analysis.

Microelectrode Array Implantation

Microelectrode implantation was performed 3 weeks before electrophysiologic recording. The mice were anesthetized

with isoflurane (3% for induction and 1.2 to 1.5% for maintenance). Each mouse was placed in a stereotaxic frame, and the dorsal fur of the head was removed using microsurgical scissors. After drying the skull with a cotton tip, a craniotomy was performed, removing a 1-mm × 2-mm section of the skull above the hippocampus (coordinates: AP −2.0 mm, ML 2 mm). Care was taken to avoid bleeding and to ensure that the dura and cortex remained intact. An HSP (Neuropixels 2.0 probe, NP2013) was slowly implanted into the hippocampus (DV 2.5 mm) through the cranial window. A 0.8-mm-diameter micro screw (Asia Bolt, South Korea) was inserted into a drilled hole in the interparietal bone above the cerebellum to serve as a reference. Both the silicon probe connector and the reference wire were secured to the skull using dental cement (C&B-Metabond, catalog no. 171032, Parkell, USA). After the surgery, the mice were group-housed for a 3-week recovery period. On the recording day, the mice were habituated for 30 min before a 10-min recording session using a specific recording system (Neuropixels, Belgium).

In Vivo Chronic Brain Recording from Awake and Restrained Mice

The mice with implanted multishank HSP were recorded chronically before and 9 h after surgery. The electrophysiologic recordings were performed using Neuropixels PXIe acquisition system (PXIe1000) and PXI-chassis (PXIe1083, National Instrumentations, USA) with standard headstage (HS_2010). The mice were head-fixed and restrained on a homemade constrainer. Recordings started when the mice were assessed to be accommodated to the headplate and lasted for 5 min. Electrophysiologic recording was made with a 30-kHz sampling rate by Open Ephys GUI[29] and open-ephys-plugins Neuropixels PXI.

Virus Injection and Cranial Window

The procedures were performed as previously outlined.[25,27,30] In brief, the mice were anesthetized with oxygenated isoflurane (3% for induction and 1.5% for maintenance) delivered in oxygen while being carefully monitored. Eye lubricant was applied to prevent corneal dehydration. The dorsal fur between the outer canthus and concha was shaved, and the mouse was positioned in a stereotactic frame with ear bars, securing the front teeth onto the incisor bar. The mouse's snout was covered with an anesthetic mask delivering oxygenated gases. The skin was prepared with povidone–iodine solution (Aplicare, Inc., USA), followed by a 70% alcohol swab (BD, USA). After infiltrating the area with lidocaine (1%, 0.2 ml), the skin over the dorsal skull was removed. A curved scalpel blade (#12) was used to remove a 3-mm × 3-mm bone flap over the left hippocampus. Using a glass needle with a diameter of about 50 μm, 1 μl of AAV8-hDlx-GCaMP6f (Vigene) and AAV8-CaMKII-jRGECO1a (Canadian Neurophotonics Platform Viral Vector Core Facility, RRID: SCR_016477) was microinjected into the left hippocampus (Bregma −2 to −2.5 mm, lateral 1.5 to 3 mm, depth 1.5 to 2 mm) using a Nanoject (Drummond Scientific Company, USA). Immediately after the injection, the visual cortex over the dorsal hippocampus was removed, following established procedures for two-photon imaging of the hippocampus as previously detailed in studies[31,32] and a 3-mm round glass cylinder topped with a 5-mm round cover slip was placed in the cranial window. The assembly was secured with adhesive luting cement (C&B Metabond). Finally, a customized metal bar was attached for stabilization during intravital two-photon imaging.

Two-photon Imaging and Data Process

After 28 days of recovery and viral transfection, the mice were acclimated to the two-photon microscope setup, with their heads restrained for 30 min each day for 3 consecutive days. Baseline imaging was performed before surgery using a Discovery laser (Coherent, USA). The laser wavelength was set to 920 nm for GCaMP6f and 1,120 nm for jRGECO1a, with an average laser power output of approximately 25 mV during imaging. A 16×, 0.8 NA water immersion objective (Olympus, Japan) was used for image acquisition, and data were collected using Prairie View Software as previously described. Additional imaging was conducted 9 h after surgery. All images were captured at a frame rate of 6.2 Hz while the mice were awake and unanesthetized. To correct for motion between frames, the NoRMCorre software package was used.[26] Neurons were subsequently selected using custom scripts in MATLAB (MathWorks). Calcium fluorescence signals from each neuron were extracted from the corrected image series. Background fluorescence changes were accounted for by subtracting them from the signal of the immediate surrounding area. The activity time course for each neuron was quantified using the formula $\Delta F = (F - F0)/F0$, where F represents the fluorescence signal at a given frame, and F0 was calculated from a sliding window of ±30 s around the frame. Baseline correction was performed by fitting a linear function (MATLAB function robustfit) to the lowpass-filtered signal (cutoff: 0.3 Hz). A deconvolution algorithm (fast online deconvolution of calcium imaging data) was applied to detect transients, with the start and end of transients identified when the model exceeded 0.1, as previously described.[33] All analysis codes are available at https://github.com/harnett/Shiqian-analysis.

Data Analysis of Electrophysiologic Recording

Raw data went through filtering, thresholding (6σ) and automatic spike sorting using SpyKING CIRCUS (version 1.0.9, https://github.com/spyking-circus/spyking-circus). Unit analyses and postprocessing were performed using spikeinterface (0.101.0)[34] and custom codes with manual curation written in Python and are

available in our laboratory's GitHub repository (https://github.com/Shenlab-MGH/spike-sorting_neuropixels2), which uses the packages NumPy (version 1.26.4, https://numpy.org), SciPy (version 1.11.3, https://scipy.org), and pandas (version 0.5.3, https://pandas.pydata.org/) for data analysis and matplotlib (version 3.9.0, https://matplotlib.org) and spikewidgets (version 0.5.4, https://github.com/SpikeInterface/spikewidgets) for visualization. Units were sorted into putative pyramidal cells and interneurons on the basis of peak waveform shape, firing rate, and interspike interval.[35,36]

Statistics and Reproducibility

To minimize potential biases, all analyses were performed in a blinded manner. The data from behavioral, electrophysiology, and calcium imaging studies are presented as means ± SD. There were no missing data for any of the behavioral test variables. For the behavioral tests, all parameters at baseline, 9 h, and 24 h were expressed as percentages relative to the baseline values within the same group. Data normality was first assessed using the Shapiro–Wilk test. Because the data were not normally distributed, logarithmic transformation was applied to normalize the variables. One-way ANOVA followed by Tukey *post hoc* analysis was then used to determine differences between groups. A significance level of $P < 0.05$ was considered statistically significant, and all tests were two-tailed. Adjusted P values were calculated using the Bonferroni correction, dividing the real P values by the number of comparisons made, and the adjusted P values are reported. Degrees of freedom for the ANOVA were calculated using the Greenhouse–Geisser correction to adjust for violations of the sphericity assumption. When comparing Z scores from baseline to 9 and 24 h after surgery, we first calculated the difference score (*i.e.*, the change from baseline) for each time point. We then compared the difference scores between the two groups using one-way ANOVA. All data points, including outliers, were retained to ensure transparency. Statistical differences were evaluated using both parametric (ANOVA test) and nonparametric (Kruskal–Wallis test) methods, and the results were concordant across approaches, confirming the robustness of our findings. All statistical analyses were performed using Prism 6 software (GraphPad Software, Inc., USA). For two-group comparisons of the electrophysiologic data, a two-sided t test was used. Electrophysiologic statistical analysis was conducted using custom codes designed to assess single-unit changes before and after surgery. The code is written in Python and is available in our laboratory's GitHub repository (https://github.com/Shenlab-MGH/spike-sorting_neuropixels2). We used the packages NumPy (version 1.26.4, https://numpy.org), SciPy (version 1.11.3, https://scipy.org), and pandas (version 0.5.3, https://pandas.pydata.org/) for data analysis and matplotlib (version 3.9.0, https://matplotlib.org) for visualization.

The sample sizes were determined based on previous studies in the field, practical considerations, and the need to detect meaningful differences in the outcomes of interest. Specifically, for the behavioral tests, the power calculation was based on data from a preliminary study conducted under the same conditions. Using these data and assuming a two-sided t test, we determined that a sample size of 10 per group would provide 95% significance. Four groups, each with N = 10 (5 males and 5 females), were used for the behavioral studies. For *in vivo* calcium imaging, a sample size of N = 4 males was selected, consistent with previous studies and sufficient to demonstrate the observed differences.[27,37,38] Due to limitations in probe cost and implantation failure rates, electrophysiologic analysis was performed using three groups of male animals (N = 2).

Results

Anesthesia/Surgery Induces Postoperative Delirium–like Behavior in Aged but Not in Adult Mice

We assessed POD-like behavior in both natural and learned behaviors by evaluating a battery of tests, including the open field, Y maze, buried food, and NOR tests, in both adult and aged mice.[27,28,39] Baseline behavioral assessments were conducted before anesthesia/surgery, followed by repeat tests 9 and 24 h postoperatively (fig. 1A). At 9 h postoperatively, anesthesia/surgery in aged mice resulted in increased latency to enter the center (78.88% *vs.* 227.3%; 95% CI, −293 to −3.918; $P = 0.013$) during the open field test ($F [2.001, 18.01] = 5.526$; fig. 1B), indicating alterations in the mice's natural behavior, including increased anxiety and changes in their natural responses. In the Y maze test, aged mice displayed fewer entries (107.6% *vs.* 60.78%; 95% CI, 0.74 to 92.94; $P = 0.005$; $F [2.351, 21.16] = 6.277$) and spent less time (94.64% *vs.* 80.38%; 95% CI, −30.63 to 59.15; $P = 0.744$; $F [1.975, 17.78] = 0.2964$) in the novel arm (fig. 1C), indicating impairments in spatial memory, which may reflect deficits in attention, consciousness, and organized thinking. Furthermore, aged mice took significantly longer to locate and consume buried food (41.29% *vs.* 135.5%; 95% CI, −182.5 to −5.893; $P = 0.004$; $F [1.820, 16.38] = 8.153$) compared to young adults (fig. 1D), suggesting disruptions in natural behavior. In the NOR test, aged mice exhibited impaired recognition memory, demonstrated by a reduced exploration time (94.94% *vs.* 68.37%; 95% CI, 1.258 to 51.88; $P = 0.007$; $F [2.045, 18.40] = 6.424$) of the novel object relative to the familiar one (fig. 1E). These abnormalities were largely resolved at 24 h postoperatively. When the behavioral indices were computed into Z score, aged mice had significantly higher Z scores (0.35 *vs.* 9.36; 95% CI, −13.55 to −4.479; $P = 0.0001$; $F [2.155, 19.40[= 27.61$) than adult mice at 9 h after surgery. However, Z scores indicated no significant differences between male

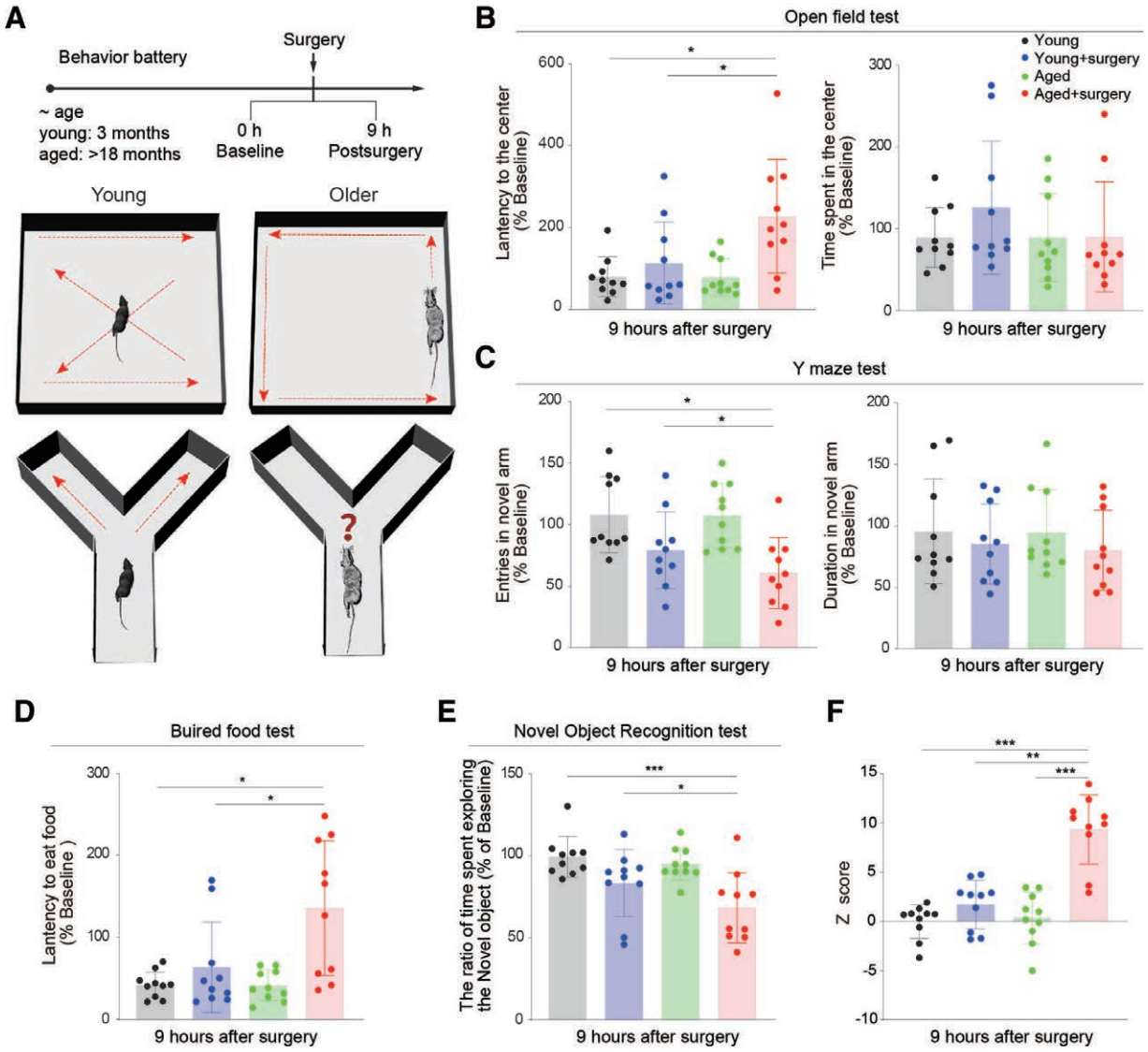

Fig. 1. Anesthesia/surgery induces postoperative delirium (POD)–like behavior in aged but not in young adult mice. (*A*) Diagram of procedures and behavioral tests (*top*) and graphic illustration of battery behavior test (*bottom*). (*B*) Comparison of young mice and aged mice on latency to the center (*left*) and the time spent in the center (*right*) of the open field test before and 9 h after the surgery. The *P* values indicate the difference in these changes between young and aged mice (n = 10, one-way ANOVA followed by Tukey *post hoc* analyses). (*C*) Comparison of young mice and aged mice on entries in the novel arm (*left*) and duration in the novel arm (*right*) of Y maze test before and 9 h after the surgery (n = 10, one-way ANOVA followed by Tukey *post hoc* analyses). (*D*) Comparison of young mice and aged mice on the latency to eat food before and 9 h after the surgery (n = 10, one-way ANOVA followed by Tukey *post hoc* analyses). (*E*) Comparison of young mice and aged mice on the ratio of time spent exploring the novel object before and 9 h after the surgery (n = 10, one-way ANOVA followed by Tukey *post hoc* analyses). (*F*) Comparison of young mice and aged mice on composite Z score in mice before and 9 h after the surgery (n = 10, one-way ANOVA followed by Tukey *post hoc* analyses). The data are means ± SD. **P* < 0.05; ***P* < 0.01; ****P* < 0.001.

and female mice (supplemental fig. S1, https://links.lww.com/ALN/D940). Z scores for both age groups at 24 h postoperatively were comparable to baseline levels, suggesting the improvement of POD-like behavior, which mirrors the fluctuating clinical course observed in human POD[40] (fig. 1F; supplemental fig. S2, https://links.lww.com/ALN/D940).

Electrophysiologic Recording from Large Neuronal Populations in the Hippocampus

We took advantage of the multishank HSP to record from the hippocampal regions. Specifically, the probes were implanted to capture neural activity across the hippocampal and cortical regions in awake, head-fixed mice (supplemental fig. S3, https://links.lww.com/ALN/D940).

Representative raw traces from the hippocampus are shown in figure 2B, illustrating local field potentials and spiking activity captured from multiple recording sites. To extract spike data, we employed a generic spike sorting toolbox, SpyKING CIRCUS,[42] which involves a generic five-step processing pipeline (fig. 2C): (1) recording extracellular potentials, (2) preprocessing raw traces with bandpass filtering (300 to 6000 Hz) and common reference subtraction, (3) spike detection using a thresholding method (6σ), (4) feature extraction and clustering, and (5) template matching to assign detected spikes to specific clusters. The representative sorted templates and auto-/cross-correlograms are plotted in supplemental figure S4 (https://links.lww.com/ALN/D940). After spike sorting, we identified distinct neuronal populations, including putative pyramidal neurons and interneurons, mapped to their respective locations along the probe (fig. 2, D and E). These sorted neurons were identified and mapped on the probe shanks, which were aligned with the Allen Brain Atlas to provide an accurate anatomical context for our recordings by measuring the distance between brain region layers and their respective angles. For the brain slice at bregma −2.06 mm, the lower boundary of the cortex and the upper boundary of the hippocampus form an 18-degree angle relative to the horizontal plane. This alignment showed that the distance between the cortex and the CA1 region was approximately 250 μm, with the 18-degree angle corresponding to the contour of the nonactive region between the cortex and CA1. This consistency with known anatomical features of the mouse brain[43] not only supports the accuracy of our probe placement but also confirms the anatomical precision of our recordings. Finally, spike rasters from the four shanks of the multishank probe

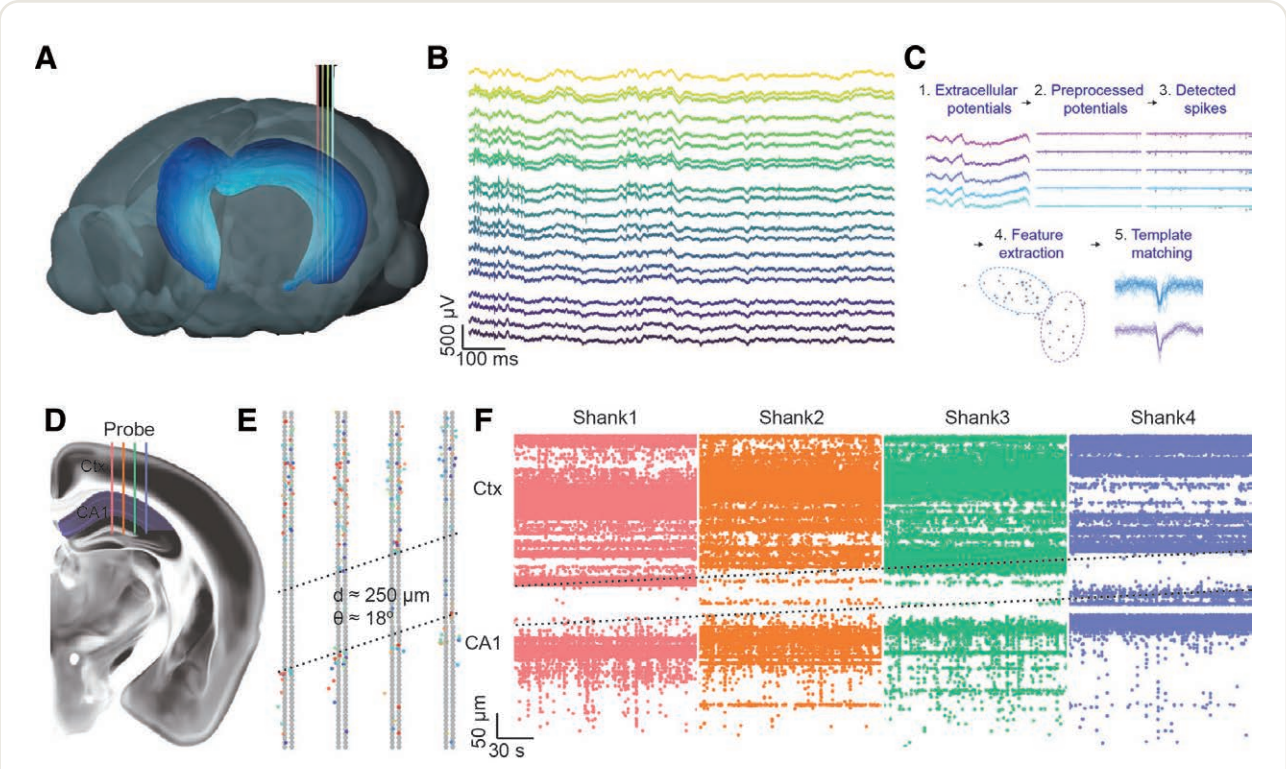

Fig. 2. Electrophysiology recording from large neuronal populations in hippocampus region in an awake head-fixed mouse. (*A*) Illustration of signals acquired from a four-shank high-density silicon probe inserted through hippocampus region. The approximate structure boundaries of four shanks are shown in four different colors. For the heat maps, each square represents a single site. (*B*) Example raw data traces show local field potentials and spiking signals recorded from 10 nearby recording sites in the hippocampus region in an awake, head-fixed mouse. (*C*) Spike sorting process of spiking signals: (1) record extracellular potentials by high-density neural probe with recording system, (2) preprocess raw traces by bandpass filter (300 to 6000 Hz) and common reference subtractions, (3) spikes are detected by thresholding (6σ) over traces, (4) assign each detected spike to a cluster by selecting and extracting features from spikes by principal component analysis, and (5) template matching process by computing similarity between any element and center of clusters. (*D*) The approximate probe implantation locations are shown overlaid on the Allen Mouse Brain Atlas (generated by BrainGlobe[41]). A total of 1,014 putative individual neurons in six animals were recorded simultaneously. (*E*) The probe map illustrates the physical locations of the recorded pyramidal neurons within the hippocampal region, with the *dotted line* indicating the boundary between the cortex (Ctx) and hippocampal CA1 regions. The distance between two regions is 250 μm with an 18-degree angle. (*F*) The example spiking raster plot presents data from a probe chronically implanted in a single mouse, capturing spike activity across 768 recording sites. Each colored block corresponds to spike times recorded from a shank with 192 channels, with the spikes plotted according to the depth along the probe where they were detected.

are presented in figure 2F. Each colored block represents spike times recorded from a shank consisting of 192 channels, plotted according to the depth along the probe where the spikes occurred. This comprehensive representation of neural activity across multiple hippocampal layers enables detailed examination of neural dynamics in both adult and aged mice, with single-neuron resolution. In summary, our results demonstrate that the high-density silicon probe can record neural activity across extensive brain regions, with the ability to specifically identify key areas such as the hippocampus from an electrophysiologic perspective.

Interneuron Hypoactivity and Pyramidal Neuron Hyperactivity Contribute to Neural Network Dysfunction in Postoperative Delirium–like Behavior

To investigate the role of neural activity implicated in POD, we first classified the spike-sorted units into three distinct neuronal types based on waveform peak-to-trough duration and the autocorrelogram τ_{rise}, following the criteria established by Petersen *et al.* (fig. 3A).[36] Each unit was plotted on a graph representing its peak-to-trough time against the autocorrelogram τ_{rise}, allowing for clear differentiation between pyramidal cells, narrow interneurons, and wide interneurons (fig. 3B). To validate the accuracy of this classification, we projected all units into a two-dimensional linear discriminant analysis space, demonstrating well-separated clusters corresponding to each neuron type (classification accuracy = 0.96). This projection confirmed the robustness of this classification method, with distinct groupings of pyramidal cells, narrow interneurons, and wide interneurons. In summary, we can cluster different neuron types, providing valuable insights for neuron-specific electrophysiologic analysis. This approach facilitates a comprehensive examination of neuronal dynamics, particularly in the context of POD within the hippocampus.

We then analyzed the spike count of these three neuron types before and after anesthesia/surgery in both adult and aged mice (fig. 3, D and E). The results indicated significant differences in neuronal activity between these two age groups. Specifically, aged mice showed an increase in hyperactive pyramidal cells (0.6 ± 2.46 Hz, $P = 0.0003$, t(225) = 2.665) and a decrease in total interneuron activity (−0.75 ± 1.99, $P = 0.0001$, t[112] = 4.009) at 9 h postoperatively, compared to adults. Notably, at 24 h postoperatively, these differences were largely diminished (supplemental fig. S5, https://links.lww.com/ALN/D940), concordant with the alleviation of POD-like behavior.

Finally, we present the statistical analysis highlighting the significant increase of hyperactive pyramidal neurons and the hypoactivity of integrated interneurons (both wide and narrow) in aged mice after anesthesia (fig. 3, F and G). The average firing rate of classified interneurons was also analyzed separately for narrow and wide interneurons (supplemental fig. S6, https://links.lww.com/ALN/D940). We also plotted a histogram of the difference between postanesthesia/surgery and preanesthesia/surgery spike counts, highlighting hypoactivity in aged mice, defined by the distance between the fitted curves of aged and adult mice (fig. 3H). These findings suggest a disrupted excitation–inhibition balance in the hippocampal network of aged mice in the early postoperative period, which may contribute to the development of POD-like behavior.

IPA Pretreatment Attenuates Postoperative Delirium–like Behavior in Aged Mice after Anesthesia/Surgery

Mitochondrial dysfunction is a key factor contributing to POD.[44,45] Repression of PGC-1α has been linked to neurodegeneration, while enhancing its expression has been shown to reverse mitochondrial dysfunction.[46,47] Building on our previous findings,[24] which highlighted the potential of IPA to enhance PGC-1α expression and protect against POD, we administered IPA to aged mice and evaluated their POD-like behavior.

Aged mice received daily IPA injections (12 mg/kg) for 14 days before anesthesia/surgery (fig. 4A). Behavioral assessments were conducted before and after the surgery, including open field, Y maze, buried food, and NOR tests. As shown in figure 4 (B through E), IPA pretreatment significantly reduced the latency in finding and eating buried food, which was markedly prolonged in control mice after surgery. This improvement suggests that IPA pretreatment alleviated some of the disruptions in natural behavior typically seen in aged mice after anesthesia/surgery.

Furthermore, IPA-pretreated mice exhibited improved performance in the Y maze, open field, and NOR tests compared to the control group, suggesting that IPA has the potential to improve cognitive function in aged mice after anesthesia/surgery. Specifically, IPA-pretreated mice showed better spatial memory, exploration, and anxiety-related behaviors, as evidenced by their increased entries into the novel arm of the Y maze (63.88% *vs.* 96.40%; 95% CI, 1.109 to 63.94; $P = 0.003$; F [1.949, 17.54] = 8.528), longer time spent in the center of the open field (128% *vs.* 115.1%; 95% CI, −88.74 to 114.5; $P = 0.662$; F [1.157, 10.41] = 0.2494), and increased exploration of the novel object in the NOR test (76.34% *vs.* 88.73%; 95% CI, 0.4713 to 24.30; $P = 0.0009$; F [1.982, 17.84[= 10.65). The significant increase in the composite Z score (1.484 *vs.* 7.214; 95% CI, −9.865 to −1.595; $P = 0.0004$; F [1.281, 11.53] = 21.00) indicates that POD-like behavior is more significant in aged mice without IPA compared to those pretreated with IPA (fig. 4F). Together, these results suggest that IPA may offer a promising preventive approach for mitigating cognitive dysfunction and POD in aging populations.

IPA Pretreatment Alleviates Electrophysiologic Alterations in Aged Mice after Anesthesia/Surgery

To assess the impact of IPA injection on neural activity changes, we recorded and analyzed electrophysiologic

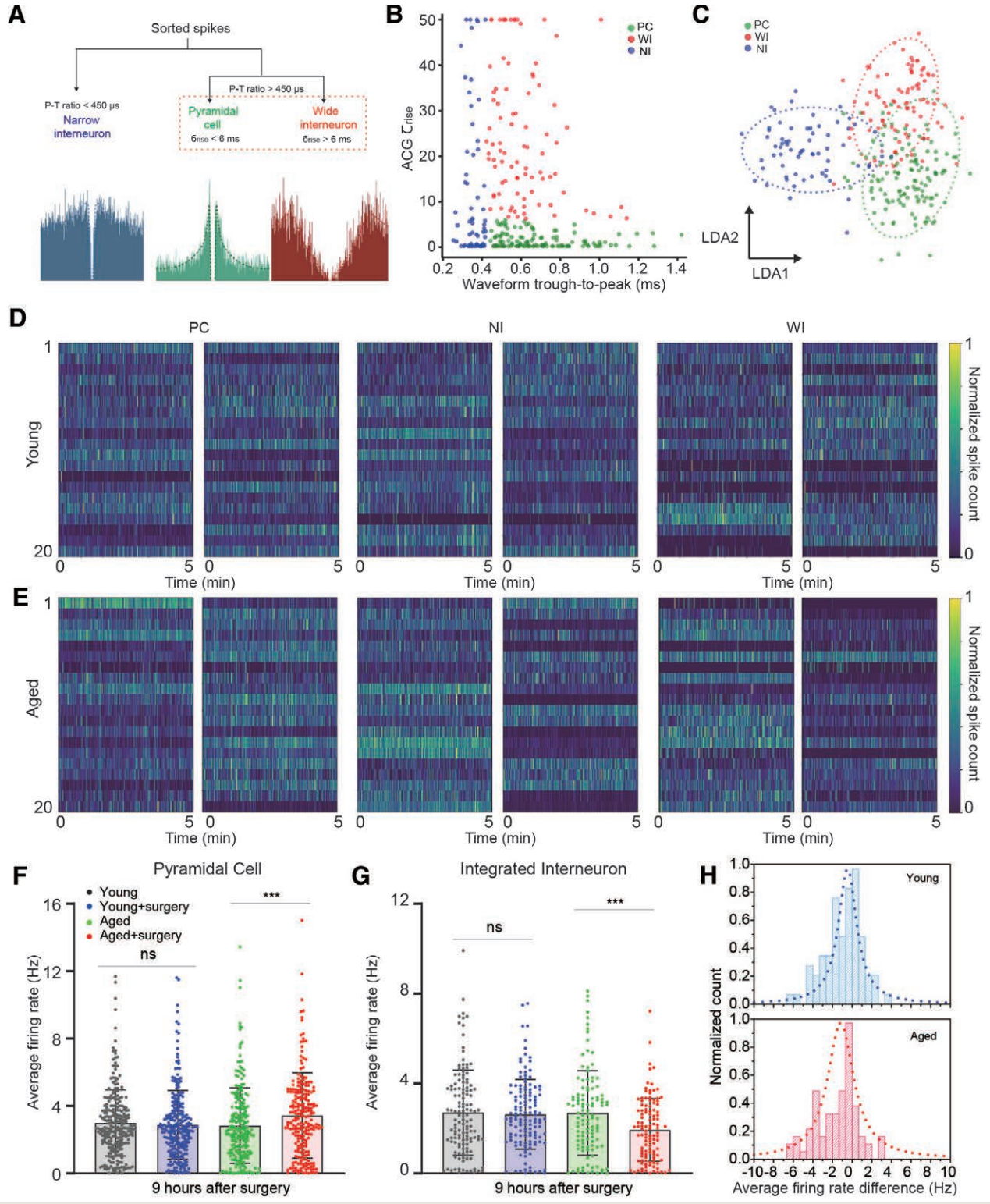

Fig. 3. Interneuron hypoactivity and pyramidal neuron hyperactivity contribute to neural network dysfunction and remote memory impairment after anesthesia/surgery. (*A*) Postprocessing step indicates the classification of pyramidal cells (PC), narrow interneurons (NI), and wide interneurons (WI) characterized by spike-waveform characterization.[36] Representative autocorrelograms show the difference of three types of neurons, with a *dotted line* representing the fitted curve to determine τ_{rise}. (*B*) Neuron-type classification based on spike-waveform width (trough-to-peak) and the temporal scale of the rising phase of the autocorrelogram (ACG; τ_{rise}).[36] (*C*) Clusters of different neuron *(Continued)*

signals in aged mice pretreated with IPA and compared them to untreated controls. We first analyzed the spike count of the three neuron types before and after anesthesia/surgery in aged mice with IPA pretreatment (figure 5A), suggesting that IPA pretreatment helps counteract the effects of anesthesia/surgery by reducing pyramidal cell hyperactivity and improving interneuron hypoactivity. Further statistical analysis indicated that, in IPA-pretreated mice, there were no significant changes in the activity of either pyramidal cells (0.029 ± 1.672, $P = 0.804$, $t(202) = 0.25$) or interneurons (0.407 ± 2.219, $P = 0.091$, $t(86) = 1.71$) when comparing pre- and postsurgery states (figure 5B and C). This suggests that IPA may help stabilize neuronal firing patterns, preventing the exaggerated activity often seen in untreated aged mice after surgery.

Additionally, we plotted a histogram showing the difference in spike count before and after anesthesia/surgery in aged mice with and without IPA pretreatment. The results revealed a notable attenuation of hypoactivity in IPA-pretreated mice, as evidenced by a smaller gap between the fitted curves for the two groups (figure 5D and E). These findings suggest that IPA pretreatment helps restore the excitation–inhibition balance in the hippocampal network of aged mice, potentially mitigating the development of POD-like behavior.

Overall, these findings are consistent with the hypothesis that IPA pretreatment prevents the excitation–inhibition imbalance within the hippocampal network of aged mice. By correcting disruptions in neural activity, IPA pretreatment may offer a potential strategy for mitigating POD-like behavior and cognitive impairments in aging populations (fig. 5).

Altered Hippocampal Neural Dynamics in Aging-associated Postoperative Delirium and Improvement with IPA Pretreatment

Our microelectrode recording data showed a decrease in interneuronal activity along with an increase in excitatory activity in the hippocampus of aged mice compared to adult mice. To further validate these findings, we used two-channel intravital two-photon calcium imaging to simultaneously examine excitatory neurons and interneurons in the hippocampus of mice undergoing anesthesia/surgery and developing POD. The neurons were labeled with green and red calcium indicators, respectively, using a well established viral strategy based on *CaMKII* and *dlx* promoters,[24,33,48] which efficiently target excitatory neurons and interneurons, respectively (fig. 6A). Specifically, AAV8-Dlx-GCaMP6f (green) and AAV8-CaMKII-jRGECO1a (red) viruses were injected into the hippocampus of mice to label the interneurons and excitatory neurons. Imaging was conducted before (0 h) and 9 h after surgery (n = 4; fig. 6B). The results showed that aged mice exhibited heightened calcium dynamics in excitatory neurons and attenuated calcium dynamics in interneurons 9 h after surgery, consistent with pyramidal neuron hyperactivity and interneuron hypoactivity captured using a high-density neural probe.

Notably, IPA pretreatment significantly improved these abnormal hippocampal neural dynamics by reducing excitatory neuron hyperactivity and enhancing interneuron activity in aged mice postoperatively (fig. 6, C through H). These findings from both calcium imaging and electrophysiologic recording implicate imbalanced neural dynamics in POD and suggest that IPA helps restore this balance to mitigate POD development.

Discussion

In this study, we investigated the impact of anesthesia and surgery on neural activity in the hippocampal region of aged mice and its association with POD-like behavior. Our results suggest a working hypothesis that delirium-like behavior in aged mice is accompanied by decreased interneuron activity and increased pyramidal neuron activity in the hippocampus. These results also revealed that IPA pretreatment could attenuate these abnormal neural activities and alleviate delirium-like behavior.

Our data indicated that anesthesia/surgery induced significant neural alterations in aged mice characterized by interneuron hypoactivity and pyramidal neuron hyperactivity. These changes in neural activity disrupted the excitation–inhibition balance within the hippocampal circuitry, the integrity of which is critical for maintaining cognitive function and memory consolidation.[49,50] The observed reductions in interneuron activity likely impaired the inhibitory control over pyramidal neurons, leading to a hyperactive state in excitatory neurons. This neural imbalance was closely associated with cognitive impairments observed in aged mice after surgery, as evidenced by their poor performance in behavioral tests such as the open field, Y maze, buried food, and NOR tests. This imbalance is consistent

Fig. 3. *(Continued)* types on low dimensional linear discriminant analysis (LDA) space span on the first two dimensions: LDA1 and LDA2. (*D*) Binned spike count of different neuron types before and after anesthesia/surgery in young mice (bin size, 1 s). (*E*) Binned spike count of different neuron types before and after anesthesia/surgery in aged mice (bin size, 1 s). (*F*) Comparison of young mice and aged mice on the average firing rate of pyramidal neurons before and 9 h after the surgery (n = 253/226 for young/aged mice, unpaired *t* test, double sided). (*G*) Comparison of young mice and aged mice on the average firing rate of integrated interneurons before and 9 h after the surgery (n = 132/113 for young/aged mice, unpaired *t* test, double sided). *$P < 0.05$; **$P < 0.01$; ns, not significant. (*H*) Histogram showing the difference in total spike count of integrated interneurons before and after anesthesia/surgery in young and aged mice. The *dotted line* represents a Lorentzian fit to the histogram data.

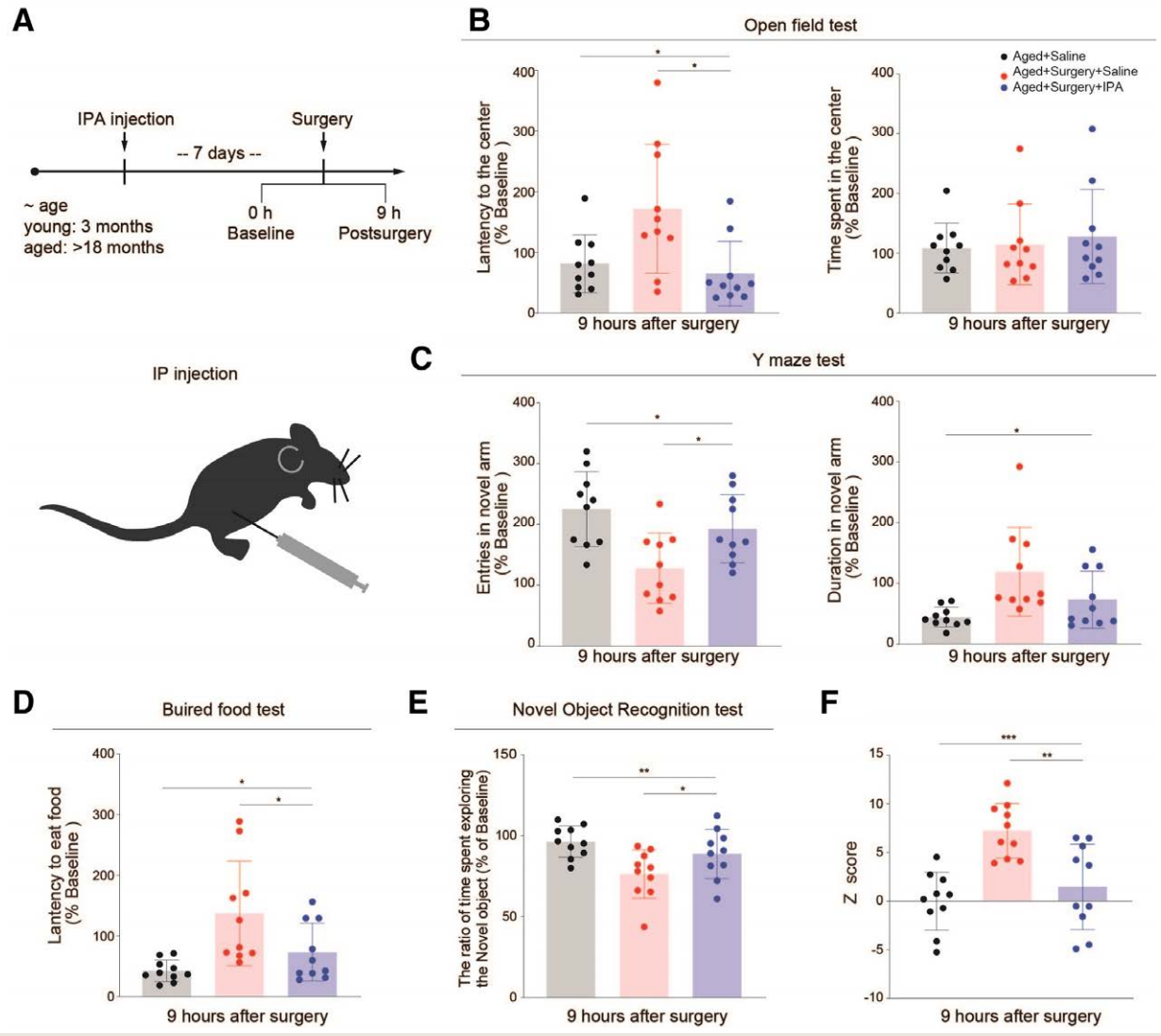

Fig. 4. IPA pretreatment ameliorates postoperative delirium (POD)–like behavior in aged mice after anesthesia/surgery. (*A*) Diagram of procedures of battery behavior test with and without indole-3-propionic acid (IPA) injection. (*B*) Comparison of aged mice with and without IPA injection, assessing the latency to enter the center (*left*) and the time spent in the center (*right*) in the open field test, both before and 9 h after the surgery. The *P* values indicate the differences in these changes between the groups of aged mice pretreated with IPA and those without the injection (n = 10, one-way ANOVA followed by Tukey *post hoc* analyses). (*C*) Comparison of aged mice with and without IPA injection, assessing the entries in the novel arm (*left*) and duration in the novel arm (*right*) of Y maze test before and 9 h after the surgery (n = 10, one-way ANOVA followed by Tukey *post hoc* analyses). (*D*) Comparison of aged mice with and without IPA injection, assessing the latency to eat food before and 9 h after the surgery (n = 10, one-way ANOVA followed by Bonferroni *post hoc* analyses). (*E*) Comparison of aged mice with and without IPA injection, assessing the ratio of time spent exploring the novel object before and 9 h after the surgery (n = 10, one-way ANOVA followed by Tukey *post hoc* analyses). (*F*) Comparison of aged mice with and without IPA injection with composite Z score before and 9 h after the surgery (n = 10, one-way ANOVA followed by Tukey *post hoc* analyses). The data are means ± SD. **P* < 0.05; ***P* < 0.01; ****P* < 0.001.

with previous studies that have shown similar dysfunctions in other brain regions during POD.[51,52] Our group has previously reported that chronic pain pushed cortical neural network into a hypersynchronous state, underpinned by interneuron hypoactivity.[37] Maintaining an intricate balance between excitation and inhibition, therefore, is of critical importance for normal neural function. A disruption of this balance is linked to the pathogenesis of many pathologic conditions, including POD.

IPA, which is known for its neuroprotective properties, has previously been shown to play a role in restoring neuronal function in various neurologic conditions.[53] In this study, IPA pretreatment was shown to reduce interneuron hypoactivity and ameliorate pyramidal neuron

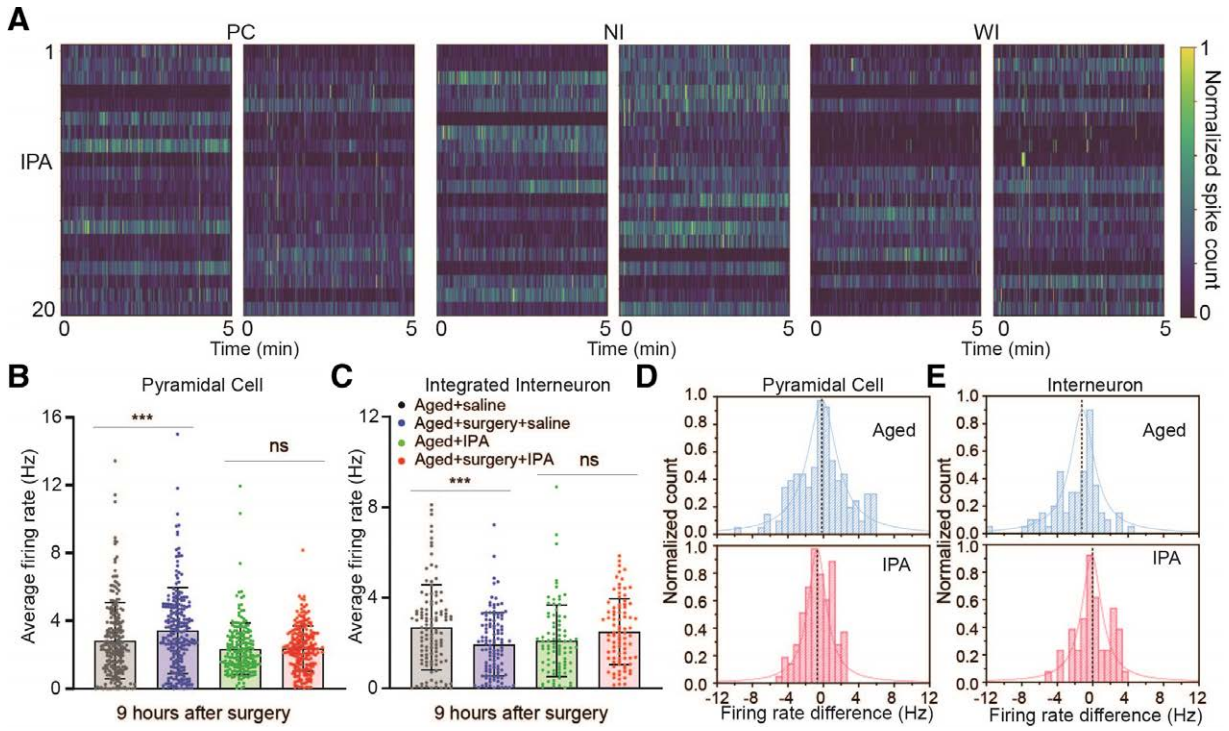

Fig. 5. Indole-3-propionic acid (IPA) pretreatment alleviates electrophysiologic alterations in aged mice after anesthesia/surgery. (*A*) Binned spike count of different neuron types (pyramidal cells [PC], narrow interneurons [NI], and wide interneurons [WI]) before and after anesthesia/surgery in IPA-injected aged mice (bin size, 1 s). (*B*) Comparison of aged mice with and without IPA injection on the average firing rate of pyramidal neurons before and 9 h after the surgery (n = 226/203 for saline/IPA-pretreated mice, unpaired *t* test, double sided). (*C*) Comparison of aged mice with and without IPA injection on the average firing rate of integrated interneurons before and 9 h after the surgery (n = 113/87 for saline/IPA-pretreated mice, unpaired *t* test, double sided). **P* < 0.05; ***P* < 0.01; ns, not significant. (*D*) Histogram showing the difference in total spike count of pyramidal neurons before and after anesthesia/surgery in aged mice with and without IPA injection. The *dotted line* represents a Lorentzian fit to the histogram data. (*E*) Histogram showing the difference in total spike count of integrated interneurons before and after anesthesia/surgery in aged mice with and without IPA injection. The *dotted line* represents a Lorentzian fit to the histogram data.

hyperactivity in aged mice after anesthesia and surgery. This aligns with previous findings demonstrating IPA's potential to enhance expression of PGC-1α, a regulator of neuronal integrity, particularly in interneurons.[24,54] Our results suggest that IPA's ability to restore the excitation–inhibition balance in the hippocampus could be a promising approach for mitigating POD-like behavior in aging animals.

To further understand the neural dynamics involved in POD, we used intravital two-photon calcium imaging to assess hippocampal neurons implicated in POD. Using previously validated methods to target excitatory neurons and interneurons, we were able to visualize neural dynamics in the hippocampus, particularly in the CA1 region, at single-neuron resolution in awake and resting mice before and after anesthesia/surgery. Our calcium imaging data corroborated the electrophysiologic findings, showing that aged mice exhibited heightened calcium activity in excitatory neurons and diminished activity in interneurons after surgery. Importantly, IPA pretreatment attenuated these neural alterations, further confirming its potential as a preventive strategy to mitigate POD-like behavior.

While our study focused on the hippocampus, a region crucial for cognitive functions such as memory, human studies investigating EEG biomarkers of POD have identified global brain network disruptions, including changes in slow-wave oscillations and cortical coherence. These EEG abnormalities suggest that similar disturbances in the excitation–inhibition balance may occur across multiple brain regions in POD patients. Although our approach, utilizing single-unit electrophysiologic recordings, differs from EEG studies in spatial resolution and scale, both methodologies emphasize the importance of disrupted neural activity in the development of POD. Our findings suggest that the hippocampal imbalance observed in aged mice may reflect similar disturbances in human POD, providing valuable insights into the neural mechanisms underlying this condition. Although our findings align with previous studies using high-density electrophysiologic recordings, the small sample size of animals might restrict the generalizability of our results. Future

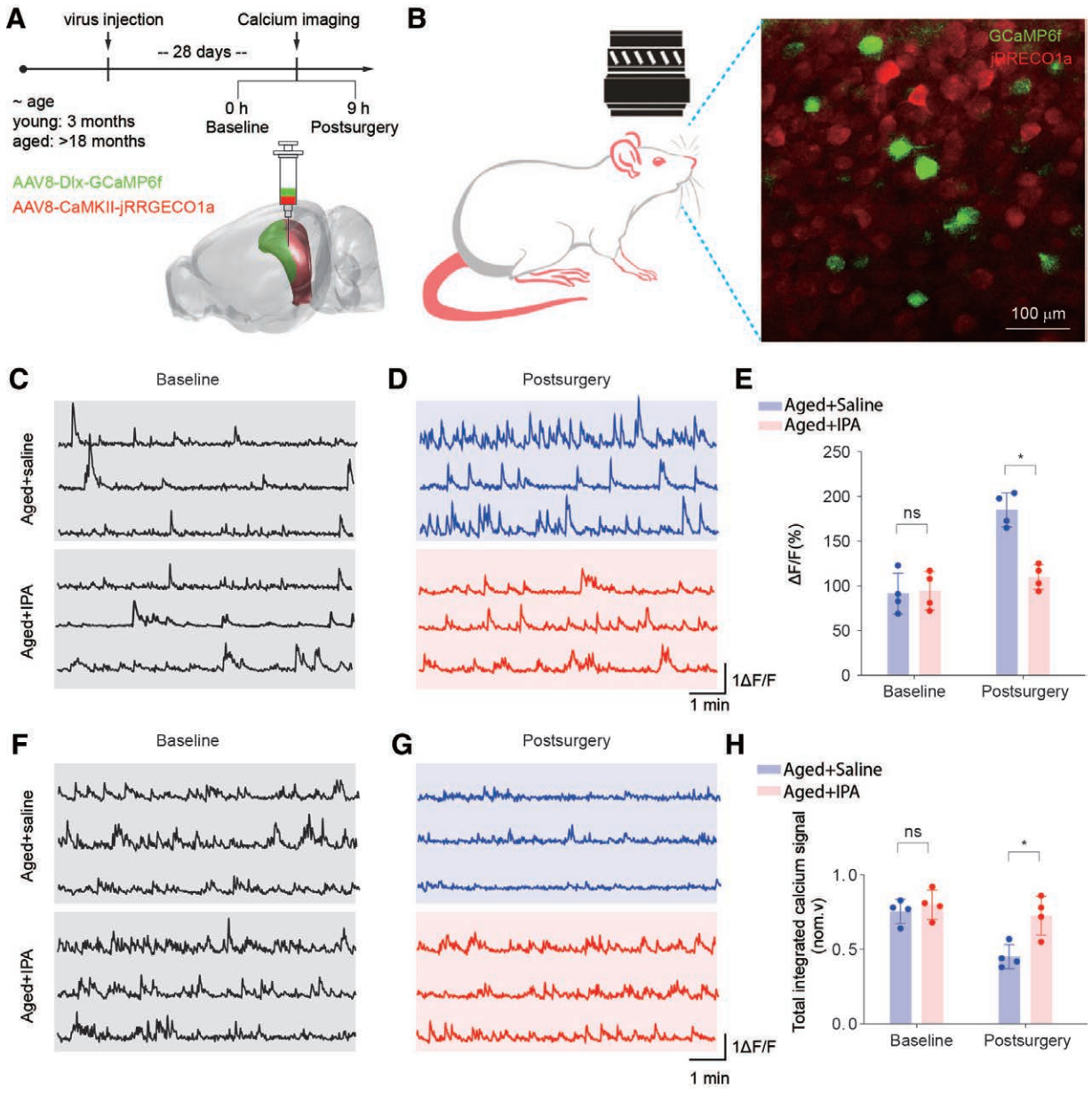

Fig. 6. Altered hippocampal neural dynamics in aging-associated postoperative delirium (POD) and improvement with indole-3-propionic acid (IPA) injection. (*A*) Flowchart and sketch depict the experimental design. AAV8-CaMKII-jRGECO1a and AAV8-Dlx-GCaMP6f were injected into the hippocampus 4 weeks ahead of the baseline imaging followed by anesthesia/surgery. (*B*) Diagram demonstrates intraviral imaging (*left*) and a representative image of GCamP6f (*green*) and jRGECO1a (*red*) expression. *Scale bar*, 100 μm. (*C* to *E*) Excitatory activity in response to anesthesia/surgery. (*C*, *D*) representative traces of excitatory neurons of hippocampus across groups. (*E*) Statistics of ΔF/F. N = 4 mice, two-way ANOVA followed by Bonferroni *post hoc* test to determine the difference among the groups. (*F* to *H*) Inhibitory activity in response to anesthesia/surgery. (*F*, *G*) representative traces of inhibitory neurons of hippocampus across groups. (*H*) Integrated calcium signal of inhibitory neurons across groups. N = 4 mice, two-way ANOVA followed by Bonferroni *post hoc* test to determine the difference among the groups. $^{*}P < 0.05$; $^{**}P < 0.01$; ns, not significant.

studies with larger cohorts are needed to strengthen these findings.

In conclusion, our study demonstrates that anesthesia/surgery induces an imbalance in hippocampal neural activity in aged mice, which might be associated with POD-like behavior. Moreover, our results indicate that IPA pretreatment attenuates the excitation–inhibition imbalance in the hippocampus, suggesting its potential as a therapeutic strategy for preventing or treating POD in aging populations. This study highlights the importance

of understanding the neural dynamics involved in POD and provides a promising avenue for future research and therapeutic interventions.

Acknowledgments

The authors thank the Massachusetts General Hospital (Charlestown, Massachusetts) Institutional Animal Care and Use Committee and the animal facility for kind support; Scot Mackeil (Senior Biomedical Electronics Technologist, Massachusetts General Hospital Bioengineer Lab) for anesthesia equipment maintenance and validation; and the Department of Anesthesia, Critical Care and Pain Medicine of Massachusetts General Hospital for generous support. The authors also thank Shelley Turok, Catherine Fong, David Duarte, and Ariel Mueller for administrative support.

Research Support

Dr. Shen's lab receives support from National Institutes of Health (Bethesda, Maryland) grant Nos. R35GM128692, R01AG070141, and R01AG082775 and National Science Foundation grant No. EAGER 2334666. Dr. Guo receives support from the National Academy of Medicine (Washington, D.C.) Healthy Longevity Global Competition Catalyst Award. Dr. Ding receives support from the Eleanor and Miles Shore Faculty Development Award (Harvard Medical School, Boston, Massachusetts).

Competing Interests

The authors declare no competing interests.

Correspondence

Address correspondence to Dr. Shen: Massachusetts General Hospital and Harvard Medical School, 149 13th Street, Charlestown, Massachusetts 02129. sshen2@mgh.harvard.edu

Supplemental Digital Content

Supplemental figures, https://links.lww.com/ALN/D940

References

1. Whitlock EL, Vannucci A, Avidan MS: Postoperative delirium. Minerva Anestesiol 2011; 77:448–56.
2. Silverstein JH, Deiner SG: Perioperative delirium and its relationship to dementia. Prog Neuropsychopharmacol Biol Psychiatry 2013; 43:108–15. doi: 10.1016/j.pnpbp.2012.11.005
3. Jin Z, Hu J, Ma D: Postoperative delirium: Perioperative assessment, risk reduction, and management. Br J Anaesth 2020; 125:492–504. doi:10.1016/j.bja.2020.06.063
4. Zywiel MG, Hurley RT, Perruccio AV, Hancock-Howard RL, Coyte PC, Rampersaud YR: Health economic implications of perioperative delirium in older patients after surgery for a fragility hip fracture. J Bone Joint Surg Am 2015; 97:829–36. doi: 10.2106/JBJS.N.00724
5. Watne LO, Idland A-V, Fekkes D, et al.: Increased CSF levels of aromatic amino acids in hip fracture patients with delirium suggests higher monoaminergic activity. BMC Geriatr 2016; 16:149. doi: 10.1186/s12877-016-0324-0
6. Sadeghirad B, Dodsworth BT, Schmutz Gelsomino N, et al.: Perioperative factors associated with postoperative delirium in patients undergoing noncardiac surgery: An individual patient data meta-analysis. JAMA Netw Open 2023;6:e2337239. doi: 10.1001/jamanetworkopen.2023.37239
7. Robinson TN, Raeburn CD, Tran ZV, Angles EM, Brenner LA, Moss M: Postoperative delirium in the elderly: Risk factors and outcomes. Ann Surg 2009; 249:173–8. doi:10.1097/SLA.0b013e31818e4776
8. Witlox J, Eurelings LSM, de Jonghe JFM, Kalisvaart KJ, Eikelenboom P, van Gool WA: Delirium in elderly patients and the risk of postdischarge mortality, institutionalization, and dementia: A meta-analysis. JAMA 2010; 304:443–51. doi:10.1001/jama.2010.1013
9. Fong TG, Davis D, Growdon ME, Albuquerque A, Inouye SK: The interface between delirium and dementia in elderly adults. Lancet Neurol 2015; 14:823–32. doi:10.1016/S1474-4422(15)00101-5
10. Marcantonio ER: Postoperative delirium: A 76-year-old woman with delirium following surgery. JAMA 2012; 308:73–81. doi:10.1001/jama.2012.6857
11. Lin L, Zhang X, Xu S, et al.: Outcomes of postoperative delirium in patients undergoing cardiac surgery: A systematic review and meta-analysis. Front Cardiovasc Med 2022; 9:884144. doi:10.3389/fcvm.2022.884144
12. Gou RY, Hshieh TT, Marcantonio ER, et al.; SAGES Study Group: One-year Medicare costs associated with delirium in older patients undergoing major elective surgery. JAMA Surg 2021; 156:430–42. doi: 10.1001/jamasurg.2020.7260
13. van der Kooi AW, Slooter AJ, van Het Klooster MA, Leijten FS: EEG in delirium: Increased spectral variability and decreased complexity. Clin Neurophysiol 2014; 125:2137–9. doi:10.1016/j.clinph.2014.02.010
14. Jacobson SA, Leuchter AF, Walter DO: Conventional and quantitative EEG in the diagnosis of delirium among the elderly. J Neurol Neurosurg Psychiatry 1993; 56:153–8. doi:10.1136/jnnp.56.2.153
15. Steggerda MJ, van den Boom F, Witteveen T, Moonen LMF: Displacement patterns of stranded I-125 seeds after permanent brachytherapy of the prostate: Dosimetry in the operating room put into perspective. Radiother Oncol 2017; 124:68–73. doi: 10.1016/j.radonc.2017.05.017
16. Pollak M, Leroy S, Röhr V, Brown EN, Spies C, Koch S: Electroencephalogram biomarkers from

anesthesia induction to identify vulnerable patients at risk for postoperative delirium. Anesthesiology 2024; 140:979–89. doi:10.1097/ALN.0000000000004929
17. Acker L, Wong MK, Wright MC, et al.; INTUIT and PRIME study groups: Preoperative electroencephalographic alpha-power changes with eyes opening are associated with postoperative attention impairment and inattention-related delirium severity. Br J Anaesth 2024; 132:154–63. doi:10.1016/j.bja.2023.10.037
18. Gjini K, Casey C, Kunkel D, et al.: Delirium is associated with loss of feedback cortical connectivity. Alzheimers Dement 2024; 20:511–24. doi:10.1002/alz.13471
19. Deschamps A, Ben Abdallah A, Jacobsohn E, et al.; Canadian Perioperative Anesthesia Clinical Trials Group: Electroencephalography-guided anesthesia and delirium in older adults after cardiac surgery: The ENGAGES-Canada randomized clinical trial. JAMA 2024; 332:112–23. doi:10.1001/jama.2024.8144
20. Steinmetz NA, Aydin C, Lebedeva A, et al.: Neuropixels 2.0: A miniaturized high-density probe for stable, long-term brain recordings. Science 2021; 372:eabf4588. doi:10.1126/science.abf4588
21. Coughlin B, Muñoz W, Kfir Y, et al.: Modified Neuropixels probes for recording human neurophysiology in the operating room. Nat Protoc 2023; 18:2927–53. doi:10.1038/s41596-023-00871-2
22. De Filippo R, Schmitz D: Differential ripple propagation along the hippocampal longitudinal axis. eLife 2023; 12:e85488. doi:10.7554/eLife.85488
23. Wikoff WR, Anfora AT, Liu J, et al.: Metabolomics analysis reveals large effects of gut microflora on mammalian blood metabolites. Proc Natl Acad Sci U S A 2009; 106:3698–703. doi:10.1073/pnas.0812874106
24. Zhou X, Wu X, Wu Y, et al.: Indole-3-propionic acid, a gut microbiota metabolite, protects against the development of postoperative delirium. Ann Surg 2023; 278:e1164–74. doi:10.1097/SLA.0000000000005886
25. Ding W, Yang L, Chen Q, et al.: Foramen lacerum impingement of trigeminal nerve root as a rodent model for trigeminal neuralgia. JCI Insight 2023; 8:e168046. doi:10.1172/jci.insight.168046
26. Wilding LA, Hampel JA, Khoury BM, et al.: Benefits of 21% oxygen compared with 100% oxygen for delivery of isoflurane to mice (Mus musculus) and rats (Rattus norvegicus). J Am Assoc Lab Anim Sci 2017; 56:148–54.
27. Yang L, Ding W, Dong Y, et al.: Electroacupuncture attenuates surgical pain-induced deliriumlike behavior in mice via remodeling gut microbiota and dendritic spine. Front Immunol 2022; 13:955581. doi:10.3389/fimmu.2022.955581
28. Peng M, Zhang C, Dong Y, et al.: Battery of behavioral tests in mice to study postoperative delirium. Sci Rep 2016; 6:29874. doi:10.1038/srep29874
29. Siegle JH, López AC, Patel YA, Abramov K, Ohayon S, Voigts J: Open Ephys: An open-source, plugin-based platform for multichannel electrophysiology. J Neural Eng 2017; 14:045003. doi:10.1088/1741-2552/aa5eea
30. Ding W, Yang L, Shi E, et al.: The endocannabinoid N-arachidonoyl dopamine is critical for hyperalgesia induced by chronic sleep disruption. Nat Commun 2023; 14:6696. doi:10.1038/s41467-023-42283-6
31. Nieh EH, Schottdorf M, Freeman NW, et al.: Geometry of abstract learned knowledge in the hippocampus. Nature 2021; 595:80–4. doi:10.1038/s41586-021-03652-7
32. Masala N, Mittag M, Giovannetti EA, et al.: Aberrant hippocampal Ca^{2+} microwaves following synapsin-dependent adeno-associated viral expression of Ca^{2+} indicators. eLife 2024; 13:RP93804. doi:10.7554/eLife.93804
33. Ding W, Fischer L, Chen Q, et al.: Highly synchronized cortical circuit dynamics mediate spontaneous pain in mice. J Clin Invest 2023; 133:e166408. doi:10.1172/JCI166408
34. Buccino AP, Hurwitz CL, Garcia S, et al.: SpikeInterface, a unified framework for spike sorting. eLife 2020; 9:e61834. doi:10.7554/eLife.61834
35. Senzai Y, Buzsaki G: Physiological properties and behavioral correlates of hippocampal granule cells and mossy cells. Neuron 2017; 93:691–704.e5. doi:10.1016/j.neuron.2016.12.011
36. Petersen PC, Siegle JH, Steinmetz NA, Mahallati S, Buzsaki G: CellExplorer: A framework for visualizing and characterizing single neurons. Neuron 2021; 109:3594–608.e2. doi:10.1016/j.neuron.2021.09.002
37. Ding W, Fischer L, Chen Q, et al.: Highly synchronized cortical circuit dynamics mediate spontaneous pain in mice. J Clin Invest 2023; 133:e166408. doi:10.1172/JCI166408
38. Kaszas A, Szalay G, Slézia A, et al.: Two-photon GCaMP6f imaging of infrared neural stimulation evoked calcium signals in mouse cortical neurons in vivo. Sci Rep 2021; 11:9775. doi:10.1038/s41598-021-89163-x
39. Yang XD, Wang LK, Wu HY, Jiao L: Effects of prebiotic galacto-oligosaccharide on postoperative cognitive dysfunction and neuroinflammation through targeting of the gut-brain axis. BMC Anesthesiol 2018; 18:177. doi:10.1186/s12871-018-0642-1
40. Imai T, Kurosawa K, Asada Y, et al.: Enhanced recovery after surgery program involving preoperative dexamethasone administration for head and neck surgery with free tissue transfer reconstruction: Single-center prospective observational study. Surg Oncol 2020; 34:197–205. doi:10.1016/j.suronc.2020.04.025
41. Claudi F, Petrucco L, Tyson A, Branco T, Margrie T, Portugues R: BrainGlobe atlas API: A common interface for neuroanatomical atlases. J Open Source Softw 2020; 5:2668. doi:10.21105/joss.02668

42. Yger P, Spampinato GL, Esposito E, et al.: A spike sorting toolbox for up to thousands of electrodes validated with ground truth recordings in vitro and in vivo. eLife 2018; 7:e34518. doi:10.7554/eLife.34518
43. Allen Institute for Brain Science: Allen brain map. Allen Institute for Brain Science. Available at: https://www.brain-map.org. Accessed October 24, 2024.
44. Hashimoto H, Nakamura K, Izumiyama N: Postoperative delirium easily develops in patients with intramitochondrial inclusion bodies in colonic neurons. Aging (Milano) 1997; 9:180–4. doi:10.1007/BF03340147
45. Lu Y, Chen L, Ye J, et al.: Surgery/anesthesia disturbs mitochondrial fission/fusion dynamics in the brain of aged mice with postoperative delirium. Aging (Albany NY) 2020; 12:844–65. doi:10.18632/aging.102659
46. Shin JH, Ko HS, Kang H, et al.: PARIS (ZNF746) repression of PGC-1alpha contributes to neurodegeneration in Parkinson's disease. Cell 2011; 144:689–702. doi:10.1016/j.cell.2011.02.010
47. Lucas EK, Dougherty SE, McMeekin LJ, et al.: PGC-1alpha provides a transcriptional framework for synchronous neurotransmitter release from parvalbumin-positive interneurons. J Neurosci 2014; 34:14375–87. doi:10.1523/JNEUROSCI.1222-14.2014
48. Wu X, Yang L, Li Z, et al.: Aging-associated decrease of PGC-1alpha promotes pain chronification. Aging Cell 2024; 23:e14177. doi:10.1111/acel.14177
49. Hijazi S, Smit AB, van Kesteren RE: Fast-spiking parvalbumin-positive interneurons in brain physiology and Alzheimer's disease. Mol Psychiatry 2023; 28:4954–67. doi:10.1038/s41380-023-02168-y
50. Cernotova D, Hruzova K, Levcik D, Svoboda J, Stuchlik A: Linking social cognition, parvalbumin interneurons, and oxytocin in Alzheimer's disease: An update. J Alzheimers Dis 2023; 96:861–75. doi:10.3233/JAD-230333
51. Chen K, Gupta R, Martín-Ávila A, Cui M, Xie Z, Yang G: Anesthesia-induced hippocampal-cortical hyperactivity and tau hyperphosphorylation impair remote memory retrieval in Alzheimer's disease. Alzheimers Dement 2024; 20:494–510. doi:10.1002/alz.13464
52. Lu J, Liang F, Bai P, et al.: Blood tau-PT217 contributes to the anesthesia/surgery-induced delirium-like behavior in aged mice. Alzheimers Dement 2023; 19:4110–26. doi:10.1002/alz.13118
53. Serger E, Luengo-Gutierrez L, Chadwick JS, et al.: The gut metabolite indole-3 propionate promotes nerve regeneration and repair. Nature 2022; 607:585–92. doi:10.1038/s41586-022-04884-x
54. Dimidschstein J, Chen Q, Tremblay R, et al.: A viral strategy for targeting and manipulating interneurons across vertebrate species. Nat Neurosci 2016; 19:1743–9. doi:10.1038/nn.4430